Fluctuating Harmonic Control Algorithm for Active Vibration Control of Helicopter Fuselage

Kai Lang, Nanjing University of Aeronautics and Astronautics, Nanjing, China
Pinqi Xia, Nanjing University of Aeronautics and Astronautics, Nanjing, China
Xiao Wang, Nanjing University of Aeronautics and Astronautics, Nanjing, China

Abstract

Active vibration control (AVC) has been successfully applied to reduce helicopter fuselage harmonic vibrations. The frequency domain algorithms widely used in the AVC owing to their simplicity, strong robustness, and ease of implementation. Although these frequency-domain methods efficiently suppress steady-state fuselage vibrations, their AVC performance degrades significantly under conditions of time-varying rotor loads. This paper introduces a novel Fluctuating Harmonic Control (FHC) algorithm designed to achieve rapid convergence and maintain high control effectiveness for helicopter fuselage AVC under time-varying loads. The principles of FHC are introduced, and its robustness and convergence speed are analyzed. Comparative simulations of a helicopter fuselage structure subjected to several time-varying rotor loads were conducted employing FHC and traditional algorithms, demonstrating that FHC exhibits better vibration environment tracking capability and achieves superior control performance under time-varying vibration conditions.

1. INTRODUCTION

The helicopter fuselage vibration is mainly generated by the rotor excitation loads which contain the blade passage frequency and its higher harmonics. The AVC methods can effectively suppress the helicopter fuselage vibration. Among these methods, the fuselage-based Active Control of Structural Response (ACSR) method minimizes the response errors by superimposing the actuation responses generated by actuators installed in the fuselage with the excitation responses generated by the rotor excitation loads (Ref. 1), and has the advantages of low control power, good control effectiveness, and no impact on airworthiness (Ref. 2).

Given the harmonic nature of fuselage vibrations, helicopter AVC typically employs frequency-domain algorithms based on Higher Harmonic Control (HHC). In HHC implementations, vibration signals are first converted from time to frequency domain by Discrete Fourier Transform (DFT), control inputs are then computed in frequency domain via optimization, and finally converted back to time domain by Inverse DFT for AVC. Patt et al. established robustness and convergence criteria for HHC, further developing a relaxed variant with a relaxation coefficient (Ref. 3). Numerical studies indicate that while relaxation coefficient improves vibration suppression, it reduces convergence speed. HHC-based algorithms depend on steady-state harmonic assumptions and DFT operations, necessitating extended control input update intervals (Ref. 4). This asynchronicity between input updates and error response sampling introduces control delays. To address this limitation, Song et al. proposed the Harmonic Synchronous Identification-Updating (HSIU) algorithm, enabling real-time harmonic coefficient identification and synchronous control input updates without DFT (Ref. 5). The effectiveness of the HSIU algorithm was validated through the AVC simulations and experiments for a helicopter fuselage driven by piezoelectric stack actuators. Kamaldar proposed an adaptive harmonic control algorithm based on time-domain sampling data (Ref. 6). The algorithm has a faster convergence speed than the HHC algorithm when there are modeling errors of the control system. Alternative time-domain feedforward approaches (e.g., filtered-x-LMS algorithms in Ref. 7 and Ref. 8) achieved real-time control without DFT but exhibited lower robustness to disturbances compared to HHC (Ref. 5).

Existing algorithms target steady-state harmonic vibration suppression. However, the helicopter fuselage vibration during real flight is not ideally steady harmonic vibration. When the flight state of helicopter changes, the rotor excitation loads will undergo a strongly time-variation, resulting in significant fuselage vibration and reducing the AVC effectiveness of these algorithms. By defining fluctuating harmonic basis functions, a novel Fluctuating Harmonic Control (FHC) algorithm is proposed in this paper for rapid and efficient AVC under strongly time-varying rotor loads. It's convergence and robustness is investigated. AVC simulations were carried out on a dynamically similar frame structure of a helicopter fuselage subjected to time-varying loads, and comparative analysis of control effect and convergence characteristics validates the superiority of the proposed FHC algorithm.

2. Principle of FHC algorithm

To address the limitation of poor vibration environment tracking capability in HHC-based algorithms caused by extended control input updating intervals or fixed update step sizes, the fluctuating harmonic control (FHC) algorithm is proposed in this paper by constructing the fluctuating harmonic basis functions based on the vibration response signals.

2.1. Fluctuating Harmonic Basis Functions

The helicopter fuselage vibration responses during steady forward flight are mainly the vibrations containing the blade passage frequency and its harmonics. At the n^{th} sampling time point, the control error response $\boldsymbol{e}_k(n)$ at the k^{th} measurement point, the harmonic control input $\boldsymbol{u}_m(n)$ of the m^{th} actuator, and the excitation response $\boldsymbol{d}_k(n)$ of the k^{th} measurement point can be expressed respectively as

$$
\begin{aligned}
\boldsymbol{e}_k(n) &= \sum_{i=1}^{I_c} a_{ki}\cos(\omega_i n\tau) + b_{ki}\sin(\omega_i n\tau) \\
\boldsymbol{u}_m(n) &= \sum_{i=1}^{I_c} c_{mi}\cos(\omega_i n\tau) + d_{mi}\sin(\omega_i n\tau) \\
\boldsymbol{d}_k(n) &= \sum_{i=1}^{I_c} e_{ki}\cos(\omega_i n\tau) + f_{ki}\sin(\omega_i n\tau)
\end{aligned} \tag{1}
$$

where τ is the sampling interval, ω_i is the i^{th} blade passage frequency, and I_c is the number of the control harmonic order.

Letting the harmonic coefficients of the control error responses at K measurement points be $\boldsymbol{\theta}(n)=\left[\boldsymbol{\theta}_1(n)^{\mathrm{T}} \quad \boldsymbol{\theta}_2(n)^{\mathrm{T}} \quad \dots \quad \boldsymbol{\theta}_K(n)^{\mathrm{T}}\right]^{\mathrm{T}}$ where $\boldsymbol{\theta}_k(n)=\left[a_{k1} \quad b_{k1} \quad a_{k2} \quad b_{k2} \quad \dots \quad a_{kI_c} \quad b_{kI_c}\right]^{\mathrm{T}}$, the harmonic coefficients of the control inputs at M actuators be $\boldsymbol{\gamma}(n)=\left[\boldsymbol{\gamma}_1(n)^{\mathrm{T}} \quad \boldsymbol{\gamma}_2(n)^{\mathrm{T}} \quad \dots \quad \boldsymbol{\gamma}_M(n)^{\mathrm{T}}\right]^{\mathrm{T}}$ where $\boldsymbol{\gamma}_m(n)=\left[c_{m1} \quad d_{m1} \quad c_{m2} \quad d_{m2} \quad \dots \quad c_{mI_c} \quad d_{mI_c}\right]^{\mathrm{T}}$, and the harmonic coefficients of the excitation responses at K measurement points be $\boldsymbol{\eta}(n)=\left[\boldsymbol{\eta}_1(n)^{\mathrm{T}} \quad \boldsymbol{\eta}_2(n)^{\mathrm{T}} \quad \dots \quad \boldsymbol{\eta}_K(n)^{\mathrm{T}}\right]^{\mathrm{T}}$ where $\boldsymbol{\eta}_k(n)=\left[e_{k1} \quad f_{k1} \quad e_{k2} \quad f_{k2} \quad \dots \quad e_{kI_c} \quad f_{kI_c}\right]^{\mathrm{T}}$, the relationship of $\boldsymbol{\theta}(n)$, $\boldsymbol{\gamma}(n)$ and $\boldsymbol{\eta}(n)$ at the n^{th} sampling time point for a linear system exists as follows:

$$
\boldsymbol{\theta}(n) = \boldsymbol{T}\boldsymbol{\gamma}(n) + \boldsymbol{\eta}(n) \tag{2}
$$

where $\boldsymbol{T} = diag\left[\boldsymbol{T}_1 \quad \boldsymbol{T}_2 \quad \cdots \quad \boldsymbol{T}_{I_c}\right]$ is the FRF matrix from the actuators to the measurement points of the control system, and $\boldsymbol{T}_i\ (i=1,2,\dots,I_c)$ is the FRF matrix at frequency ω_i as follows:

$$
\begin{aligned}
\boldsymbol{T}_i &= \begin{bmatrix} \boldsymbol{T}_{11}(\omega_i) & \boldsymbol{T}_{12}(\omega_i) & \cdots & \boldsymbol{T}_{1M}(\omega_i) \\ \boldsymbol{T}_{21}(\omega_i) & \boldsymbol{T}_{22}(\omega_i) & \cdots & \boldsymbol{T}_{2M}(\omega_i) \\ \vdots & \vdots & \ddots & \vdots \\ \boldsymbol{T}_{K1}(\omega_i) & \boldsymbol{T}_{K2}(\omega_i) & \cdots & \boldsymbol{T}_{KM}(\omega_i) \end{bmatrix} \\
\boldsymbol{T}_{km}(\omega_i) &= \begin{bmatrix} \mathrm{Re}(H_{km}(\omega_i)) & \mathrm{Im}(H_{km}(\omega_i)) \\ -\mathrm{Im}(H_{km}(\omega_i)) & \mathrm{Re}(H_{km}(\omega_i)) \end{bmatrix}
\end{aligned} \tag{3}
$$

where Re and Im respectively represent the real and imaginary parts of a complex number, and $H_{km}(\omega_i)$ is the value of FRF from the m^{th} actuator to the k^{th} measurement point at frequency ω_i.

Defining the harmonic basis function be $\boldsymbol{z}(n)$ = [$\sin(\omega_1 n\tau)$ $\cos(\omega_1 n\tau)$ $\sin(\omega_2 n\tau)$ $\cos(\omega_2 n\tau)$ ... $\sin(\omega_{I_c} n\tau)$], Eq. (1) can be converted into the products of the harmonic basis function and the harmonic coefficients as follows:

$$
\begin{aligned}
e_k(n) &= \boldsymbol{z}(n)^{\mathrm{T}} \cdot \boldsymbol{\theta}_k(n) \\
u_m(n) &= \boldsymbol{z}(n)^{\mathrm{T}} \cdot \boldsymbol{\gamma}_m(n) \\
d_k(n) &= \boldsymbol{z}(n)^{\mathrm{T}} \cdot \boldsymbol{\eta}_k(n)
\end{aligned} \tag{4}
$$

To effectively control the fluctuations in the vibration responses caused by time-varying loads, the fluctuation factor of the i^{th} order harmonic basis function is defined as

(5) $$\upsilon_{ki}(n) = \frac{1}{n_\upsilon}\sum_{p=1}^{n_\upsilon}\eta_{ki}(n-p)$$
$$\upsilon_i(n) = \frac{1}{K}\sum_{k=1}^{K}\upsilon_{ki}(n)$$

where n_υ is the number of samples of the excitation responses, which is for reducing the fluctuation error of the harmonic basis function caused by the error of harmonic coefficient of a single excitation response. Defining $\boldsymbol{\upsilon} = diag[\upsilon_1\ \upsilon_1\ \upsilon_2\ \upsilon_2 \ldots \upsilon_{I_c}\ \upsilon_{I_c}]$ as the fluctuation factor matrix of the harmonic basis function, the fluctuating harmonic basis function can be defined as follows:

(6) $$\hat{\boldsymbol{z}}(n) = \boldsymbol{\upsilon}\cdot\boldsymbol{z}(n)$$

Therefore, the harmonic coefficients of the control error responses and control inputs can be expressed respectively as

(7) $$\boldsymbol{\theta}(n) = \boldsymbol{\upsilon}\hat{\boldsymbol{\theta}}(n)$$
$$\boldsymbol{\gamma}(n) = \boldsymbol{\upsilon}\hat{\boldsymbol{\gamma}}(n)$$

where $\hat{\boldsymbol{\theta}}$ and $\hat{\boldsymbol{\gamma}}$ are the harmonic coefficients of the control error responses and control inputs based on the fluctuating harmonic basis function, respectively. The control error response is transformed to

(8) $$\boldsymbol{e}(n) = \hat{\boldsymbol{z}}(n)^{\mathrm{T}}\hat{\boldsymbol{\theta}}(n) + \hat{\boldsymbol{\varepsilon}}(n)$$

where $\hat{\boldsymbol{\varepsilon}}$ is the identification error vector of the control error response based on the fluctuating harmonic basis function.

The RLS method is used to identify the harmonic coefficients of the control error responses based on the fluctuating harmonic basis function. The exponential weighted least-square objective function is defined as follows:

(9) $$J\left(\hat{\boldsymbol{\theta}}\right) = \sum_{p=1}^{n}\lambda^{n-p}\left[\boldsymbol{e}(p) - \hat{\boldsymbol{z}}^{\mathrm{T}}(p)\hat{\boldsymbol{\theta}}(p)\right]^{\mathrm{T}}\left[\boldsymbol{e}(p) - \hat{\boldsymbol{z}}^{\mathrm{T}}(p)\hat{\boldsymbol{\theta}}(p)\right]$$

where $\lambda(\leq 1)$ is the forgetting factor, which is for reducing the influence of earlier data on parameter estimation. Based on the minimized objective function, the least-square solution for the harmonic coefficients of the control error responses is obtained as follows:

(10) $$\hat{\boldsymbol{\theta}}(n) = \left(\hat{\boldsymbol{z}}_n\boldsymbol{\lambda}_n\hat{\boldsymbol{z}}_n^{\mathrm{T}}\right)^{-1}\hat{\boldsymbol{z}}_n\boldsymbol{\lambda}_n\boldsymbol{e}_n$$

where $\boldsymbol{\lambda}_n = diag\left(1, \lambda^1, \ldots, \lambda^{n-1}\right)$, $\hat{\boldsymbol{z}}_n = \left[\hat{\boldsymbol{z}}(n)\quad \hat{\boldsymbol{z}}(n-1)\quad \ldots\quad \hat{\boldsymbol{z}}(1)\right]^{\mathrm{T}}$, and $\boldsymbol{e}_n = \left[\boldsymbol{e}(n)\quad \boldsymbol{e}(n-1)\quad \ldots\quad \boldsymbol{e}(1)\right]^{\mathrm{T}}$.

Letting $\boldsymbol{P}(n) = \left(\hat{\boldsymbol{z}}_n\boldsymbol{\lambda}_n\hat{\boldsymbol{z}}_n^{\mathrm{T}}\right)^{-1}$, the RLS recursive equations for the harmonic coefficients of the control error responses and the excitation responses based on the fluctuating harmonic basis function can be established as follows:

(11) $$\begin{aligned}
\boldsymbol{K}(n+1) &= \frac{\boldsymbol{P}(n)\hat{\boldsymbol{z}}(n+1)}{\lambda + \hat{\boldsymbol{z}}^{\mathrm{T}}(n+1)\boldsymbol{P}(n)\hat{\boldsymbol{z}}(n+1)} \\
\hat{\boldsymbol{\theta}}(n+1) &= \hat{\boldsymbol{\theta}}(n) + \boldsymbol{K}(n+1)\left[\boldsymbol{e}(n+1) - \hat{\boldsymbol{z}}^{\mathrm{T}}(n+1)\hat{\boldsymbol{\theta}}(n)\right] \\
\boldsymbol{P}(n+1) &= \lambda^{-1}\boldsymbol{P}(n) - \lambda^{-1}\boldsymbol{K}(n+1)\hat{\boldsymbol{z}}^{\mathrm{T}}(n+1)\boldsymbol{P}(n) \\
\boldsymbol{\eta}(n+1) &= \boldsymbol{\upsilon}\hat{\boldsymbol{\theta}}(n+1) - \boldsymbol{T}\boldsymbol{\upsilon}\hat{\boldsymbol{\gamma}}(n)
\end{aligned}$$

Combining Eq.(5), and Eq.(11), the fluctuating harmonic basis function can be updated at each sampling time point, and the harmonic coefficients of the control error responses and the excitation responses can be identified.

2.2. Control Input Harmonic Coefficient Updating

The vector of harmonic coefficients of control error responses based on the fluctuating harmonic basis functions by HHC can be expressed as

(12) $$\hat{\boldsymbol{\theta}}(n) = \boldsymbol{T}\hat{\boldsymbol{\gamma}}(n) + \boldsymbol{\upsilon}^{-1}\boldsymbol{\eta}(n)$$

where $\hat{\boldsymbol{\gamma}}(n)$ is the vector of harmonic coefficients of control inputs based on the fluctuating harmonic basis functions. A quadratic control objective function based on the fluctuating harmonic basis functions is established as follows:

(13) $$\hat{J} = \frac{1}{2}\left(\hat{\boldsymbol{\theta}}^{\mathrm{T}}\boldsymbol{W}_{\mathrm{e}}\hat{\boldsymbol{\theta}} + \hat{\boldsymbol{\gamma}}^{\mathrm{T}}\boldsymbol{W}_{\mathrm{u}}\hat{\boldsymbol{\gamma}}\right)$$

Using the steepest descent method, the updating formula of the vector $\hat{\boldsymbol{\gamma}}(n)$ is obtained as

(14) $$\hat{\boldsymbol{\gamma}}(n) = (\boldsymbol{I} - \mu\boldsymbol{W}_{\mathrm{u}})\hat{\boldsymbol{\gamma}}(n-1) - \mu\boldsymbol{T}^{\mathrm{T}}\boldsymbol{W}_{\mathrm{e}}\hat{\boldsymbol{\gamma}}(n)$$

where μ is the harmonic updating step size.

2.3. Robustness Analysis of FHC

In practical AVC of a helicopter fuselage, the modeling errors of the control system, changes in flight conditions, nonlinearities of the control system and so on will inevitably cause the identification errors of the FRF matrix, leading to decrease of control effectiveness or even control divergence. Thus the robustness of the FHC algorithm is analyzed as follows.

When there are no modeling errors, the convergence condition of Eq. (14) is that the spectral radius of the matrix $\boldsymbol{I}-\left(\boldsymbol{W}_{\mathrm{u}}+\boldsymbol{T}^{\mathrm{T}}\boldsymbol{W}_{\mathrm{e}}\boldsymbol{T}\right)$ is less than 1. Since the weighting coefficient matrices $\boldsymbol{W}_{\mathrm{e}}$ and $\boldsymbol{W}_{\mathrm{u}}$ are usually chosen as positive definite real diagonal matrices, $\boldsymbol{W}_{\mathrm{u}}+\boldsymbol{T}^{\mathrm{T}}\boldsymbol{W}_{\mathrm{e}}\boldsymbol{T}$ is a positive definite real symmetric matrix, and its eigenvalues are all positive real numbers. Therefore, the necessary condition for the convergence of FHC is

$$0<\mu<\frac{2}{\lambda_{\max}} \tag{15}$$

where $\lambda_{\max}$ is the maximum eigenvalue of the matrix $\boldsymbol{W}_{\mathrm{u}}+\boldsymbol{T}^{\mathrm{T}}\boldsymbol{W}_{\mathrm{e}}\boldsymbol{T}$.

According to Eq. (14), the harmonic coefficients of the control inputs will converge to the following optimal value:

$$\boldsymbol{\gamma}_{\mathrm{opt}}=-\left(\boldsymbol{W}_{\mathrm{u}}+\boldsymbol{T}^{\mathrm{T}}\boldsymbol{W}_{\mathrm{e}}\boldsymbol{T}\right)^{-1}\boldsymbol{T}^{\mathrm{T}}\boldsymbol{W}_{\mathrm{e}}\boldsymbol{\eta} \tag{16}$$

Then the objective function of optimal control converges to

$$J^{\mathrm{opt}}=\frac{1}{2}\boldsymbol{\eta}^{\mathrm{T}}\left[\boldsymbol{W}_{\mathrm{e}}-\boldsymbol{W}_{\mathrm{e}}\boldsymbol{T}\left(\boldsymbol{W}_{\mathrm{u}}+\boldsymbol{T}^{\mathrm{T}}\boldsymbol{W}_{\mathrm{e}}\boldsymbol{T}\right)^{-1}\boldsymbol{T}^{\mathrm{T}}\boldsymbol{W}_{\mathrm{e}}\right]\boldsymbol{\eta} \tag{17}$$

When there is an error $\Delta\boldsymbol{T}$ in the FRF matrix of the control system, the updating equation for the harmonic coefficients of the control inputs in FHC becomes

$$\boldsymbol{\gamma}(n)=(\boldsymbol{I}-\mu\boldsymbol{W}_{\mathrm{u}})\boldsymbol{\gamma}(n-1)-\mu\hat{\boldsymbol{T}}^{\mathrm{T}}\boldsymbol{W}_{\mathrm{e}}\boldsymbol{\theta}(n) \tag{18}$$

Substituting Eq. (2) into Eq. (18) yeilds:

$$\boldsymbol{\gamma}(n)=(\boldsymbol{I}-\mu\boldsymbol{W}_{\mathrm{u}}-\mu\hat{\boldsymbol{T}}^{\mathrm{T}}\boldsymbol{W}_{\mathrm{e}}\boldsymbol{T})\boldsymbol{\gamma}(n-1)-\mu\hat{\boldsymbol{T}}^{\mathrm{T}}\boldsymbol{W}_{\mathrm{e}}\boldsymbol{\eta} \tag{19}$$

The convergence condition of HSIU is that the spectral radius of matrix $\boldsymbol{I}-\mu\left(\boldsymbol{W}_{u}+\hat{\boldsymbol{T}}^{\mathrm{T}}\boldsymbol{W}_{e}\boldsymbol{T}\right)$ is less than 1, i.e.,

$$\left|1-\mu\cdot\lambda_{l}\left(\boldsymbol{W}_{\mathrm{u}}+\hat{\boldsymbol{T}}^{\mathrm{T}}\boldsymbol{W}_{\mathrm{e}}\boldsymbol{T}\right)\right|<1 \tag{20}$$

where $\lambda_{l}\left(\boldsymbol{W}_{\mathrm{u}}+\hat{\boldsymbol{T}}^{\mathrm{T}}\boldsymbol{W}_{\mathrm{e}}\boldsymbol{T}\right)$ represents the l^{th} eigenvalue of matrix $\boldsymbol{W}_{\mathrm{u}}+\hat{\boldsymbol{T}}^{\mathrm{T}}\boldsymbol{W}_{\mathrm{e}}\boldsymbol{T}$. Letting $\hat{\lambda}_{l}=\hat{\sigma}_{l}+i\hat{\varsigma}_{l}$ be the eigenvalue of matrix $\boldsymbol{W}_{\mathrm{u}}+\hat{\boldsymbol{T}}^{\mathrm{T}}\boldsymbol{W}_{\mathrm{e}}\boldsymbol{T}$, for the control convergence, the following conditions must be satisfied:

$$\begin{cases}\hat{\sigma}_{l}>0\\ 0<\mu<\dfrac{2\hat{\sigma}_{l}}{\hat{\sigma}_{l}^{2}+\hat{\varsigma}_{l}^{2}}\end{cases}\quad\left(l=1,2,\ldots,L,\ L=\min\left(K,M\right)\right) \tag{21}$$

Thus, one of the necessary conditions for FHC control convergence is that all the eigenvalues of matrix $\boldsymbol{W}_{u}+\hat{\boldsymbol{T}}^{\mathrm{T}}\boldsymbol{W}_{e}\boldsymbol{T}$ have positive real parts.

According to Eq. (19), under the condition of convergence, the harmonic coefficients of control inputs in FHC will converge to

$$\hat{\boldsymbol{\gamma}}_{\mathrm{opt}}=-\left(\hat{\boldsymbol{T}}^{\mathrm{T}}\boldsymbol{W}_{\mathrm{e}}\boldsymbol{T}+\boldsymbol{W}_{\mathrm{u}}\right)^{-1}\hat{\boldsymbol{T}}^{\mathrm{T}}\boldsymbol{W}_{\mathrm{e}}\boldsymbol{\eta} \tag{22}$$

Substituting Eq. (22) into Eq. (2), the control error responses converge to

$$\hat{\boldsymbol{\theta}}_{\mathrm{opt}}=-\boldsymbol{T}\left(\hat{\boldsymbol{T}}^{\mathrm{T}}\boldsymbol{W}_{\mathrm{e}}\boldsymbol{T}+\boldsymbol{W}_{\mathrm{u}}\right)^{-1}\hat{\boldsymbol{T}}^{\mathrm{T}}\boldsymbol{W}_{\mathrm{e}}\boldsymbol{\eta}+\boldsymbol{\eta} \tag{23}$$

And the corresponding control objective function converges to

$$\hat{J}_{\mathrm{opt}}=\frac{1}{2}\boldsymbol{\eta}^{\mathrm{T}}\left[\boldsymbol{W}_{\mathrm{e}}-\hat{\boldsymbol{\Psi}}^{\mathrm{T}}\boldsymbol{T}^{\mathrm{T}}\boldsymbol{W}_{\mathrm{e}}-\left(\hat{\boldsymbol{\Psi}}^{\mathrm{T}}\boldsymbol{T}^{\mathrm{T}}\boldsymbol{W}_{\mathrm{e}}\right)^{\mathrm{T}}+\hat{\boldsymbol{\Psi}}^{\mathrm{T}}\boldsymbol{\Gamma}\hat{\boldsymbol{\Psi}}\right]\boldsymbol{\eta} \tag{24}$$

where $\hat{\boldsymbol{\Psi}}=\boldsymbol{T}\left(\hat{\boldsymbol{T}}^{\mathrm{T}}\boldsymbol{W}_{\mathrm{e}}\boldsymbol{T}+\boldsymbol{W}_{\mathrm{u}}\right)^{-1}\hat{\boldsymbol{T}}^{\mathrm{T}}\boldsymbol{W}_{\mathrm{e}}$.

Note that the following inequality holds:

$$\begin{aligned}\boldsymbol{W}_{\mathrm{e}}\boldsymbol{T}\boldsymbol{\Gamma}^{-1}\boldsymbol{T}^{\mathrm{T}}\boldsymbol{W}_{\mathrm{e}}\geq\boldsymbol{W}_{\mathrm{e}}\boldsymbol{T}\hat{\boldsymbol{\Gamma}}^{-1}\hat{\boldsymbol{T}}^{\mathrm{T}}\boldsymbol{W}_{\mathrm{e}}+\left(\boldsymbol{W}_{\mathrm{e}}\boldsymbol{T}\hat{\boldsymbol{\Gamma}}^{-1}\hat{\boldsymbol{T}}^{\mathrm{T}}\boldsymbol{W}_{\mathrm{e}}\right)^{\mathrm{T}}\\ -\left(\hat{\boldsymbol{\Gamma}}^{-1}\hat{\boldsymbol{T}}^{\mathrm{T}}\boldsymbol{W}_{\mathrm{e}}\right)^{\mathrm{T}}\boldsymbol{\Gamma}\left(\hat{\boldsymbol{\Gamma}}^{-1}\hat{\boldsymbol{T}}^{\mathrm{T}}\boldsymbol{W}_{\mathrm{e}}\right)\end{aligned} \tag{25}$$

According to Equations (17), (24) and (25), the following inequality holds:

$$\hat{J}_{\mathrm{opt}}\geq J_{\mathrm{opt}} \tag{26}$$

which indicates that when there are modeling errors of the control system, the harmonic control objective function cannot be smaller than that without modeling errors. Particularly, if there are no restrictions on the control inputs, i.e., $\boldsymbol{W}_{\mathrm{u}}=0$, and the number of actuators in the control system is equal to the number of measurement points, i.e., $M = K$, the harmonic control objective function converges to that without modeling errors, and the harmonic coefficients of the control error responses converges to 0.

3. AVC SIMULATIONS

3.1. Dynamically similar frame structure of a helicopter fuselage

To validate vibration control performance of the FHC algorithm, AVC simulations were conducted on a 1:3 scaled dynamically similar frame structure of a helicopter fuselage driven by piezoelectric stack actuators as shown in Figure 1. The reference helicopter has an empty weight of 5000 kg, a five-bladed rotor, and a blade passage frequency of $N_{\mathrm{b}}\Omega = 25.5\mathrm{Hz}$. The dynamically similar frame structure is designed to obtain similar dynamic characteristics as the reference helicopter (detailed in Ref. 9), with two piezoelectric actuators installed on each gearbox strut. Four accelerometers are installed at four positions where the instrument panel and pilot seats are located. The rotor excitation loads including three forces (F_x , F_y , F_z) and three moments (M_x , M_y M_z) are applied at the hub center of rotor.

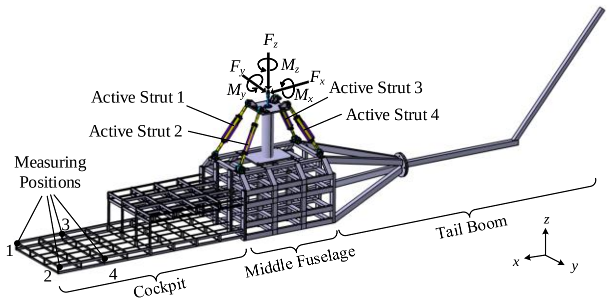

Figure 1: AVC system of dynamic similar frame structure of helicopter fuselage

3.2. AVC Simulations under Sinusoidal Time-Varying Loads

To compare the AVC effects of the FHC and traditional HHC and HSIU algorithms under the time-varying loads, AVC simulations of the helicopter fuselage structure were conducted. To simulate the time-varying loads, the rotor excitation loads at 25.5Hz were applied to the hub, and their fluctuating amplitudes were set as:

$$F_{x0}\left(n\right) = \left[1 - A_{\mathrm{f}}\sin\left(2\pi\omega_{\mathrm{f}} n\tau\right)\right]60\ \mathrm{N},$$

$$F_{y0}\left(n\right) = [1 - A_{\mathrm{f}}\sin(\omega_{\mathrm{f}} n\tau)]60\ \mathrm{N},$$

$$F_{z0}\left(n\right) = [1 - A_{\mathrm{f}}\sin(\omega_{\mathrm{f}} n\tau)]300\ \mathrm{N},$$

$$M_{x0}\left(n\right) = [1 - A_{\mathrm{f}}\sin(\omega_{\mathrm{f}} n\tau)]10\ \mathrm{N}\cdot\mathrm{m},$$

$$M_{y0}\left(n\right) = [1 - A_{\mathrm{f}}\sin(\omega_{\mathrm{f}} n\tau)]10\ \mathrm{N}\cdot\mathrm{m},$$

$$M_{z0}\left(n\right) = [1 - A_{\mathrm{f}}\sin(\omega_{\mathrm{f}} n\tau)]20\ \mathrm{N}\cdot\mathrm{m},$$

respectively, where A_{f} is the fluctuation ratio of the amplitudes, and ω_{f} is the fluctuation frequency of the amplitudes.

Figures 2~4 show the Root Mean Squares (RMSs) of control error responses of the four measurement points using HHC, HSIU, and FHC algorithms under three kinds of sinusoidal time-varying loads with the fluctuation ratios and frequencies of 25% and 0.25Hz, 50% and 0.25Hz, and 50% and 0.5Hz, respectively. Due to the amplitude fluctuation of the three time-varying loads, the AVC effects of HHC and HSIU algorithms are poor, with the response RMS suppression rates of 84.91%, 84.58%, and 69.57% for HHC, and 88.95%, 87.72%, and 75.73% for HSIU, respectively. However, the FHC algorithm, due to using fluctuating harmonic basis functions to track the fluctuation of the three time-varying loads, achieves excellent AVC effects of 98.62%, 97.90%, and 95.70%. Comparing Figures 2 and 3, it can be seen that when the fluctuation frequency increases from 0.25Hz to 0.5Hz and the fluctuation ratio keeps 25%, the response RMS suppression rates of HHC decreases from 84.91% to 84.58% by 0.33%, the response RMS suppression rates of HSIU decreases from 88.95% to 87.72% by 1.23%, and the AVC effect of FHC decreases from 98.62% to 97.90% by 0.72%. Therefore, when the fluctuation ratio keeps a constant, increasing the fluctuation frequency has a small effect on the AVC effects of the three algorithms. Comparing Figures 3 and 4 indicates that increasing the fluctuation of amplitudes significantly reduces the AVC effects of HHC and HSIU. When the fluctuation ratio increases from 25% to 50% and the fluctuation frequency keeps 0.5Hz, the response RMS suppression rates of HHC decreases from 84.58% to 69.57% by 15.01%, and the response RMS suppression rates of HSIU decreases from 87.72% to 75.73% by 11.99%. The AVC effect of FHC remains significant. Under all the three load conditions, the control effect of HSIU is better than that of HHC. It is obvious that the real-time control input updating of HSIU has a stronger vibration suppression capability under time-varying loads. However, FHC can maintain excellent vibration control effects under various load conditions, indicating that it has excellent vibration environment tracking capability.

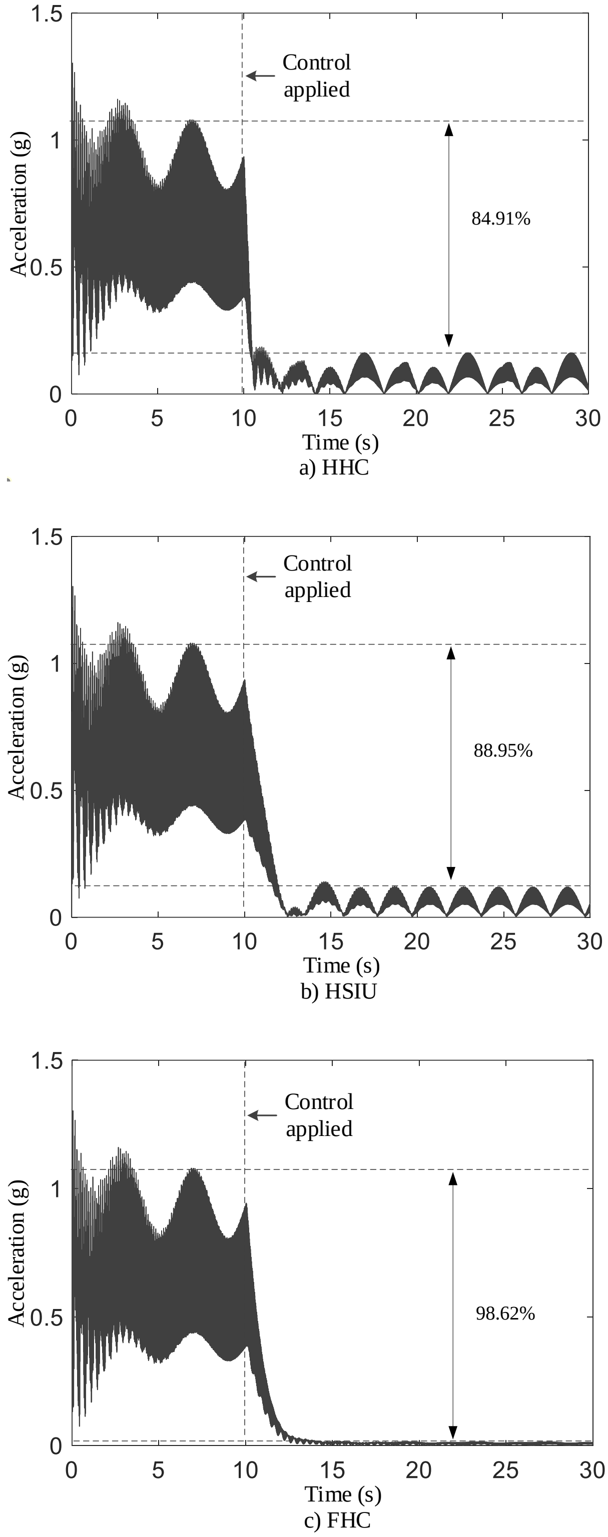

Figure 2: RMS of fuselage responses before and after AVC with a) HHC, b) HSIU and c) FHC algorithms under sinusoidal time-varying loads with $A_{\mathrm{f}} = 25\%$ and $\omega_{\mathrm{f}} = 0.25\ \mathrm{Hz}$

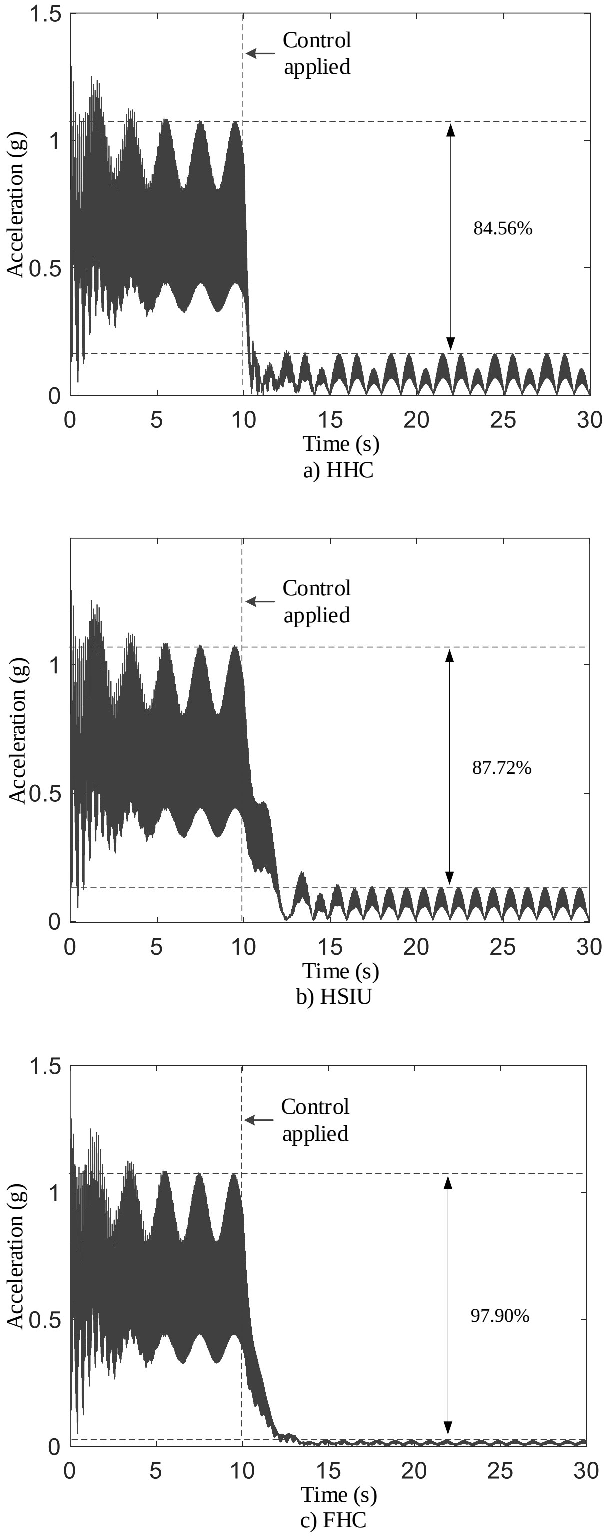

Figure 3: RMS of fuselage responses before and after AVC with a) HHC, b) HSIU and c) FHC algorithms under sinusoidal time-varying loads with $A_{\mathrm{f}} = 25\%$ and $\omega_{\mathrm{f}} = 0.5\ \mathrm{Hz}$

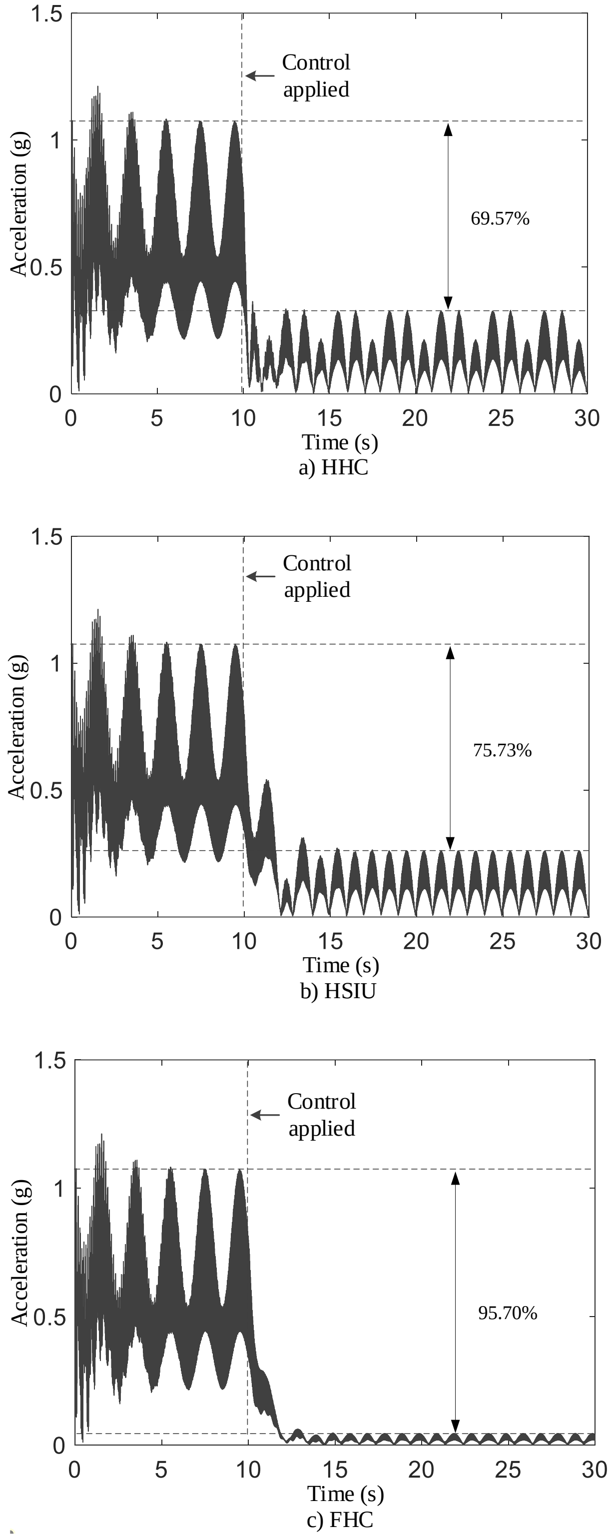

Figure 4: RMS of fuselage responses before and after AVC with a) HHC, b) HSIU and c) FHC algorithms under sinusoidal time-varying loads with $A_f = 50\%$ and $\omega_f = 0.5$ Hz

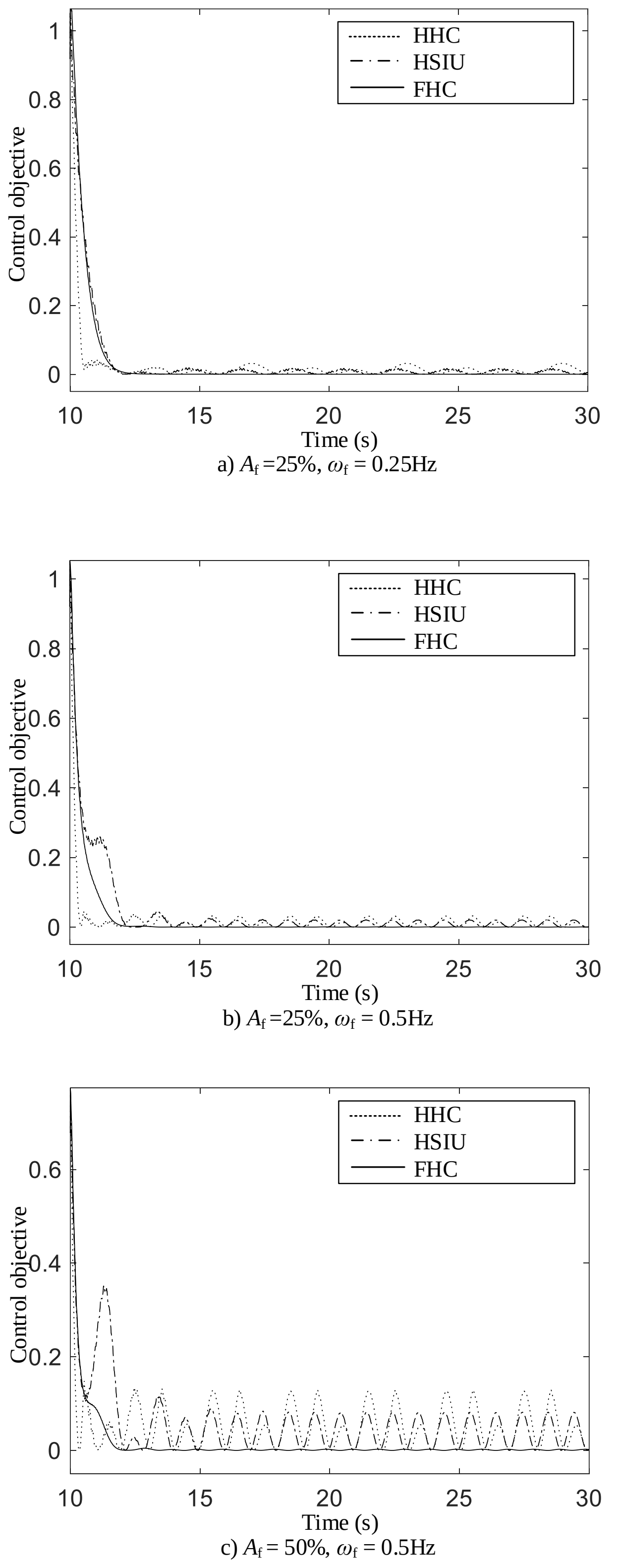

Figure 5: Time histories of objective functions during AVC with HHC, HSIU and FHC algorithms under sinusoidal time-varying loads with three groups of A_f and ω_f

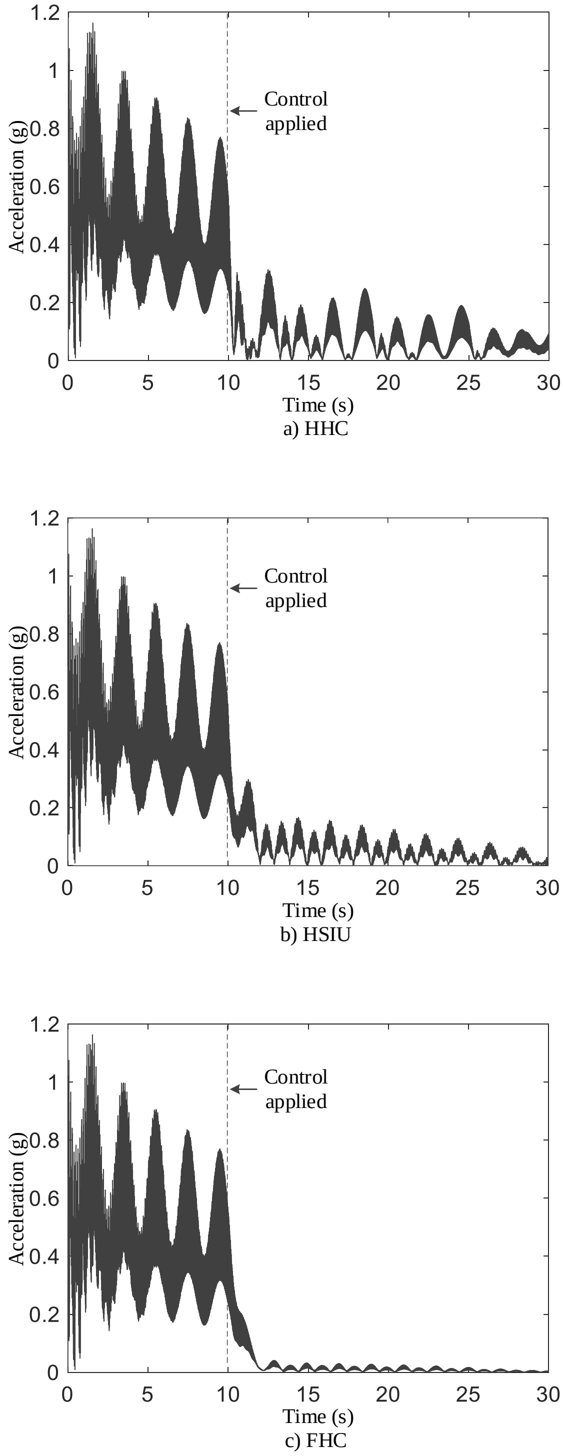

Figure 6: RMS of fuselage responses before and after AVC with a) HHC, b) HSIU and c) FHC algorithms under mixed time-varying loads

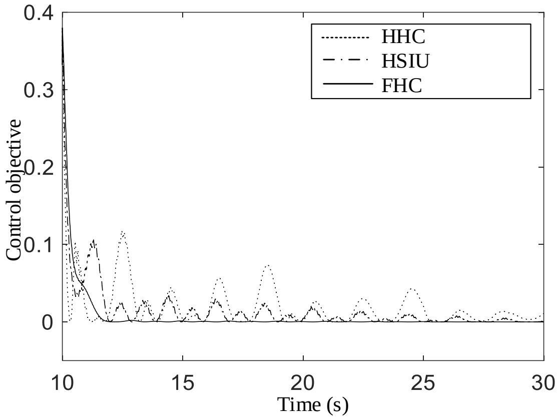

Figure 7: Time histories of objective functions during AVC with HHC, HSIU and FHC algorithms under mixed time-varying loads

Figure 5 shows the time histories of objective functions during AVC with HHC, HSIU and FHC algorithms under sinusoidal time-varying loads with three groups of A_f and ω_f. It can be seen that the convergence speed of the objective function of HHC is fastest, while HSIU and FHC show similar convergence speed. This is because control inputs of HHC update directly to the optimal values, while control inputs of HSIU and FHC update along the negative direction of the gradient of the objective function. However, the convergence values of HHC and HSIU are large, indicating that both algorithms have poor control performances under sinusoidal time-varying loads. The control objective function of HSIU converge to smaller values than HHC, which is consistent with the comparison results of the response RMS suppression rates of the two algorithms. The objective function of FHC converges to a small convergence value, indicating that FHC has excellent control performance under sinusoidal time-varying loads.

When the excitation loads are linear and sinusoidal time-varying, which is called the mixed time-varying loads, the AVC simulations of the helicopter fuselage structure were conducted adopting HHC, HSIU and FHC algorithms to further analyze their AVC ability in complex vibration environments. The amplitudes of the mixed time-varying loads are supposed as $F_{x0}(n) = v_1(n) \cdot 60 s_\mathrm{f}\,\mathrm{N}$, $F_{y0}(n) = v_1(n) \cdot 60 s_\mathrm{f}\,\mathrm{N}$, $F_{z0}(n) = v_1(n) \cdot 300 s_\mathrm{f}\,\mathrm{N}$, $M_{x0}(n) = v_1(n) \cdot 10 s_\mathrm{f}\,\mathrm{N \cdot m}$, $M_{y0}(n) = v_1(n) \cdot 10 s_\mathrm{f}\,\mathrm{N \cdot m}$, $M_{z0}(n) = v_1(n) \cdot 20 s_\mathrm{f}\,\mathrm{N \cdot m}$, where $v_1(n) = 1 - 0.9 \times n\tau/30$ is the linear time-varying coefficient, which means the amplitudes are linearly reduced to 10% of the initial values in 30s. The fluctuation ratio and fluctuation frequency of the amplitudes keep a constant of $A_{\mathrm{f}} = 50\%$ and $\omega_{\mathrm{f}} = 0.5\mathrm{Hz}$ respectively.

Figure 6 compares the RMSs of control error responses of the four measurement points using HHC, HSIU and FHC algorithms under the mixed time-varying loads. The response RMSs of HHC and HSIU have significant fluctuations after convergence to a steady-state value, and the steady-state values are very large. The response RMS of FHC has significant fluctuations at the beginning of control, but the fluctuations quickly decay to a small value, indicating that FHC still has strong AVC ability and effect under the mixed time-varying loads. Figure 7 shows the time histories of the objective function values during AVC with HHC, HSIU and FHC algorithms under the mixed time-varying loads. Similar to the case of sinusoidal time-varying loads, the convergence speed of the objective function of HHC is fastest, while HSIU and FHC show similar convergence speed. However, The objective function values of HHC and HSIU are very large after convergence to a steady-state value, while that of FHC is very small, indicating again that FHC still has excellent AVC effect under the mixed time-varying loads.

4. CONCLUSIONS

Introducing the fluctuating harmonic basis functions into the HSIU algorithm, the FHC algorithm for AVC of helicopter fuselages under time-varying loads has been proposed in this paper. AVC simulations on a dynamically similar frame structure of a helicopter fuselage driven by piezoelectric stack actuators show that the FHC algorithm has better vibration environment tracking ability and better control effect compared to traditional frequency-domain algorithms. The specific conclusions are drawn as follows:

1. Under sinusoidal time-varying loads, the increase of the fluctuation ratios and frequencies of the amplitudes will reduce the AVC effect. Due to the delay of control input of HHC, the AVC effect of HHC is the worst among the HHC, HSIU and FHC algorithms.
2. HSIU has better AVC effect than HHC under sinusoidal time-varying loads as it updates control inputs in real time. The convergence speed of HSIU is slower than HHC because HHC update control inputs directly to the optimal values.
3. The fluctuating harmonic basis functions of FHC can effectively track the fluctuations of the time-varying loads, thus FHC and efficiently suppress the fuselage vibration responses under strongly time-varying rotor loads.

Author contact:

Kai Lang langkai@nuaa.edu.cn

Pinqi Xia xiapq@nuaa.edu.cn

5. ACKNOWLEDGMENTS

This study has been supported by the Foundation of the National Key Laboratory of Helicopter Aeromechanics (Funding No. 2023-HA-LB-067-02), the Natural Science Foundation of Jiangsu Province (Grant No. BK20241373), and Technology Development Project (XYZX 060302)

6. REFERENCES

1. King, S. P., and Staple, A. E., “Minimization of Vibration Through Active Control of Structural Response,” Rotorcraft Design Operations, CP - 423, AGARD, 1986, pp. 14.1-14.13.
2. Cribbs, R. C., Friedmann, P. P., and Chiu, T., “Coupled helicopter rotor/flexible fuselage aeroelastic model for control of structural response,” AIAA Journal, Vol. 38, No.10, 2000, pp. 1777-1788.
3. Patt, D., Liu, L., Chandrasekar, J., Bernstein, D. S., and Friedmann, P. P., “Higher-Harmonic-Control Algorithm for Helicopter Vibration Reduction Revisited,” Journal of Guidance, Control and Dynamics, Vol. 28, No. 5, 2005, pp. 918–930.
4. Kamaldar, M., Hoagg, J. B., “Adaptive harmonic steady-state control for rejection of sinusoidal disturbances acting on a completely unknown system,” International Journal of Adaptive Control and Signal Processing, Vol. 31, No. 9, 2017, pp. 1308-1326.
5. Song, L., and Xia, P., “A Harmonic Synchronous Identification-Updating Method for Active Control of Helicopter Structural Response Driven by Piezoelectric Stack Actuators,” Journal of the American Helicopter Society, Vol. 60, No. 3, 2015, pp. 1-14.
6. Kamaldar, M., Hoagg J. B., “Adaptive harmonic control for rejection of sinusoidal disturbances acting on an unknown system,” IEEE

Transactions on Control Systems Technology, Vol. 28, No. 2, 2020, pp. 277- 290.

7. Hugin, C. T., Hatch, C., and Shingle, G. W., "Active Vibration Control of the Lynx Helicopter Airframe," AIAA 2007-2222, 48th AIAA/ASME/ASCE/AHS/ASC Structures, Structural Dynamics, & Materials Proceedings, Hoholulu, HI, April 23–26, 2007.

8. Hoffmann, F., Konstanzer, P., and Priems, M., "Active Cabin Vibration Reduction for Jet-Smooth Helicopter Ride," Society for Aeronautics and Astronautics 35th European Rotorcraft Forum Proceedings, Hamburg, September 22–25, 2009.

9. Lang, K., Shang L., and Xia P., "Active vibration control of helicopter fuselage with large dynamic modeling errors," *AIAA Journal*, Vol. 60, No. 3, 2022, pp. 1895-1908.